Multiphoton Transitions in a Spin-Polarized 3D Optical Lattice

A. Hemmerich, C. Zimmermann, and T. W. Hänsch
Sektion Physik der Universität München, Schellingstrasse 4/III, D-80799 München, Germany
and Max-Planck-Institut für Quantenoptik, D-85748 Garching, Germany
(Received 7 July 1993; revised manuscript received 13 October 1993)

We have observed novel resonances occurring at subharmonic frequencies in probe transmission spectra of ultracold atoms confined in the antinodes of a 3D optical standing wave by means of dipole forces. We interpret these resonances in terms of multiphoton Raman transitions between vibrational states of the trapped atoms.

PACS numbers: 32.80.Pj, 42.65.−k

Lattices of ultracold atoms trapped by dipole forces in the antinodes of three-dimensional light fields represent a unique new state of matter [1–5]. The atoms (sparsely) populate a regular lattice of microscopic light traps and thus form a very dilute "solid." The atomic motion inside each trap is quantized on a submicron length scale. The interaction of such matter with radiation involves many unusual aspects and offers intriguing opportunities for future research. Here we demonstrate a novel high-order multiphoton phenomenon that can be observed at very low power levels, opening a new regime for studies in nonlinear spectroscopy and nonlinear optics.

Much attention has recently been paid to understanding the absorption spectra of "optical lattices" [1,3–6]. Unique resonances with extremely narrow linewidth have been observed in such spectra and have been interpreted as due to Raman transitions between quantized vibrational states of the cold atoms moving inside nearly harmonic potential wells. More specifically, stimulated Raman transitions between vibrational states are excited by the cooperation of the three-dimensional trapping field (3D-field) and a probe laser beam which is directed through the trapped atomic sample. This yields amplification or attenuation of the probe beam if its detuning from the 3D-field frequency equals the frequency separation between a pair of vibrational states. In a classical picture, the interference between the probe wave and the 3D field produces a time-dependent perturbation of the optical potential which oscillates at the difference frequency between the two optical fields. When this distortion becomes resonant, transitions between vibrational states are excited [6]. In addition to these spectral features a central resonance of less than a kHz linewidth has been observed in such spectra [3,5]. According to the one-dimensional theory presented in Ref. [7] this resonance should mainly result from stimulated Rayleigh scattering. We believe that in three dimensions the formation of a Bragg grating might be responsible for the extreme narrowness of that resonance [5]. Even though only two different 3D-field geometries have so far been reported [3,5], the preceding interpretations seem to apply quite generally and thus absorption spectra of these so-called "optical crystals" or "optical lattices" may have appeared to be sufficiently well understood. However, spectroscopic experiments with increased resolution and signal to noise show novel spectral features in absorption spectra of 3D optical lattices which have not been reported and studied yet. In this paper we aim to describe these additional resonances and interpret them in terms of a new kind of multiphoton process.

We use here a new 3D-field geometry which leads to cubic body-centered optical lattices with ferromagnetically ordered atomic spins. To form this 3D optical lattice we employ the 2D field used in Ref. [4] in the x-y plane. This field consists of two mutually orthogonal 1D optical standing waves directed along the x and y axes both linearly polarized parallel to the x-y plane. As is discussed in Ref. [4], for 90° time phase difference between the two 1D waves, this geometry yields circularly polarized antinodes which form a square lattice of lines parallel to the z axis spaced by $\lambda/2$ (where $\lambda = 780$ nm is the optical wavelength). To create a 3D extension we add a circularly polarized standing wave along the z axis. This leads to a 3D cubic λ-sized lattice of pointlike circularly polarized antinodes. In contrast to the experimental situation in Refs. [4] and [5] all atomic spins in our experiment are oriented along the z axis forming a "ferromagnetic" order.

To produce the 3D field experimentally, we use the spatially filtered output beam of a grating stabilized diode laser. The frequency of the laser is detuned with respect to the $(F=3, m=3) \rightarrow (F=4, m=4)$ transition of ^{85}Rb by $\delta = -\delta\Gamma$ where Γ is the linewidth of the transition. The output beam is split into three mutually orthogonal components superposed inside a rubidium-vapor cell. Each of the beams is retroreflected by a highly reflecting mirror, thus yielding a standing wave. In other words, our setup consists of two nested Michelson interferometers. By controlling the optical path lengths between the two beam splitters employed and the three mirrors we can adjust the time phase differences between the three standing waves. We couple 1 mW in a 6 mm ($1/e^2$) diameter beam into the x and the y wave and 0.5 mW into the z wave. When the time phase difference ϕ between the x and the y wave is 90° the 3D field acquires circularly polarized antinodes which are arranged on different types of cubic lattices depending on the time-phase differences ψ between the x and the z wave. In

Fig. 1 the two characteristic cases are shown which occur for $\psi=0°$ and $\psi=90°$. In the experiment described here the values of ϕ and ψ are servo-controlled to the values $\phi=90°$ and $\psi=0°$. Error signals are obtained by analyzing the light reflected from the two nested interferometers. We thus produce a body-centered-cubic lattice of circularly polarized antinodes [as depicted on the left of Fig. 1(a)] and the spring constant of the trap potential is isotropic near an antinode. The antinode Rabi frequency is $\omega_{1\,\max}=6\Gamma$.

A cold (below 20 μK) dense (10^{10} atoms/cm^3) cloud of atoms is prepared by a magneto-optical trap operating in a rubidium-vapor cell at a few 10^{-8} Torr. The cloud is about 0.8 mm in diameter and contains approximately 10^7 atoms. The trap is active for 100 ms. Then, the trapping light and the magnetic field are switched off for a probing period of 10 ms, while the repumping laser (which counteracts hyperfine pumping) is kept active. During this time the atoms are confined by the 3D field. Our apparatus does not allow us to measure the temperature of the atoms after thermalization inside the 3D field which should occur within the first few hundred microseconds and we should expect several vibrational states to be populated. A linearly polarized (parallel to the xy plane) probe laser beam of 0.4 μW power and 0.28 mm ($1/e^2$) diameter (i.e., $\omega_{\text{probe}}/\Gamma=0.3$) is directed through the atomic sample. This beam travels within the x-y plane and is tilted only by a small angle of 5° with respect to the x axis. Its frequency ν_{probe} is tuned across the frequency of the 2D field ν_{2D} during the probing period, while its transmission through the atomic sample is recorded. The observation time has been chosen to be as short as 10 ms to guarantee a nearly constant value of the trapped atomic population within a few percent during observation. The $1/e$ decay time of the trapped population is about half a second, limited only by collisions with the rubidium background vapor.

In Fig. 2 we show a typical probe transmission spectrum. The predominant features are the resonances observed at probe frequency detunings of $\pm$ 165 kHz showing gain in the low frequency component and absorption in the high frequency component. According to previous work these resonances result from Raman transitions between adjacent vibrational states. A second pair of such Raman sidebands due to transitions involving two vibrational quanta occurs at about $\pm$ 310 kHz, i.e., at the edge of the spectrum shown in Fig. 2(a). We observe a considerably higher ratio of second to first sideband amplitude and a linewidth broadening (approximately by a factor 2) in both sidebands compared to the case when a weak probe beam (0.04 μW) is used, indicating that the

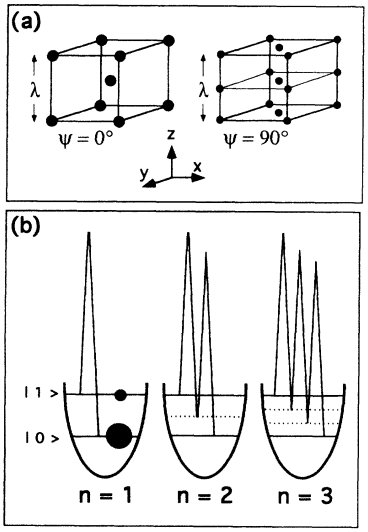

FIG. 1. (a) Crystalline structures showing the spatial arrangement of the microscopic light traps for two characteristic values of the time-phase difference ψ between the x and z wave. The spins of the trapped atoms are oriented along the z axis. Larger dots indicate deeper traps. The experiment uses the body-centered-cubic case on the left. (b) Schematic of energy conservation in multiphoton Raman transitions between vibrational states of atoms confined by an optical potential. The black dots indicate the atomic population. See text for details.

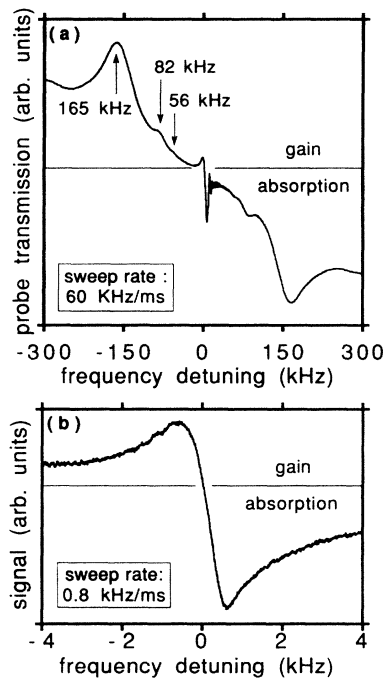

FIG. 2. (a) Recordings of the probe transmission versus the detuning between the probe and 3D-field frequency. The probe polarization is adjusted to be parallel to the x-y plane. The frequency resolution is limited by the high sweep rate which causes the fringes on the right of the central resonance. The resonances at $\pm$ 82 and $\pm$ 56 kHz result from multiphoton Raman transitions involving 4 and 6 photons in lowest order. (b) Fraction of the spectrum in (a) showing the central Rayleigh resonance recorded with much lower sweep rate.

stronger probe beam in the new experiment increases the temperature of the atoms. The width of the first Raman sideband is about 40 kHz if the weak probe beam is used.

A central resonance occurs within a few kHz away from zero detuning of the probe frequency, which is not properly resolved in the spectrum of Fig. 2(a) because of the high sweep rate used, as can be seen from the fringes on the right of this feature. These fringes result from a transient heterodyning of the decaying Rayleigh resonance with the off-resonant probe wave [5]. The sweep rate of 60 kHz/ms is determined by the 10 ms observation time used to record such spectra. In Fig. 2(b) a much smaller portion of the spectrum is recorded with a sweep rate of only 0.8 kHz/ms showing a dispersive resonance with less than 1 kHz linewidth. Such Rayleigh resonances have been observed in previous work; however, no spectrum of this resonance with comparable resolution has been reported so far. The frequency resolution in Fig. 2(b) is limited to about 200 Hz by the observation time. The stability of the probe frequency detuning is below 10 Hz for 1 s observation time. The shape of this resonance is not Lorentzian, indicating that different relaxation times are involved in its formation. In particular note the asymmetry with respect to the zero of the frequency axis which is not yet explained.

We now consider the additional structure occurring in the spectrum in Fig. 2(a) in the region between ± 100 and ± 20 kHz. We clearly recognize an additional pair of resonances at ± 82 kHz and possibly a second one at ± 56 kHz as well. To investigate these resonances we have recorded the probe transmission between -100 and 100 kHz and have subtracted a Lorentzian fit of the Raman part of the spectrum which consists of the two well understood pairs of Raman sidebands at ± 165 and ± 310 kHz. The result is plotted in Fig. 3(a), clearly confirming the existence of at least two further pairs of sidebands at ± 82 and ± 56 kHz. In the center of Fig. 3(a) the Rayleigh resonance is repeated which due to its extreme narrowness produces the transient oscillatory behavior seen on the right of the resonance. To further exploit the information in our experimental data we have smoothed the spectrum of Fig. 3(a) in the region between -100 and -25 kHz and replotted the result as the solid line in Fig. 3(b). We readily recognize a further resonance at -42 kHz in this graph. The dashed line in Fig. 3(b) represents the second derivative of the solid line clearly confirming the resonance at -42 kHz and indicating an additional resonance at about -33 kHz. In summary, we observe resonances at probe frequency detunings ν_n which approximately follow the relation $\nu_n = 165$ kHz$/n$ where $n=1$ corresponds to the first Raman sideband at 165 kHz, $n=2$ to the resonance at ± 82 kHz, and so forth.

We can interpret our observations in terms of multiphoton transitions between adjacent vibrational states. In Fig. 1(b) we sketch how such processes can give rise to the observed resonances at frequencies ν_n for $n=1,2,3$. In this picture we show only the lowest order process which contributes to each transition occurring at the subharmonic frequencies $\nu_n = \nu/n$, where $h\nu$ is the energy separation of a pair of vibrational levels indicated by $|0\rangle$ and $|1\rangle$. For the transition at frequency ν_n at least n probe photons and n pump photons (i.e., photons contributed by the 3D field) are required. Higher-order contributions to this transition can involve $n+2i$, $i=1,2,\ldots$ probe photons and $n+2j$, $j=1,2,\ldots$ probe photons. However, all orders contributing to the same resonance exchange the same net amount of photons between the pump waves and the probe. Since the lower state has higher population at thermal equilibrium the net effect is excitation of the atom from the lower to the upper state and we obtain amplification at $-\nu/n$ and absorption at $+\nu/n$ in the probe transmission signal. In the following we call the transition which is resonant at frequency ν_n the $(n-1)$st subharmonic. For $n=1$ we obtain the ordinary Raman transition.

The perturbative approach sketched above is helpful to understand the subharmonic resonance frequencies; however, it seems not well suited to estimate transition rates because both the probe and the pump waves have relatively high intensity in the experiment. We have investi-

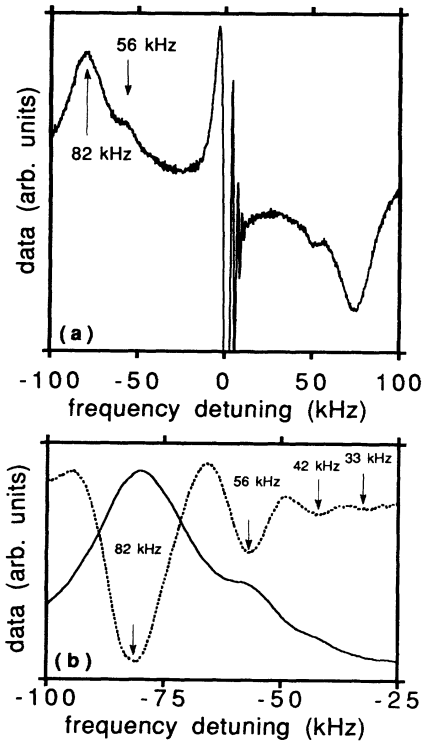

FIG. 3. (a) A fraction of the spectrum in Fig. 2(a) is shown after subtracting a Lorentzian fit of the ordinary Raman sidebands at ± 165 and ± 310 kHz. (b) The solid line repeats a smoothed fraction of the spectrum shown in (a). The dashed line is the second derivative of the solid curve. The arrows indicate the resonance frequencies of the multiphoton Raman transitions involving 4, 6, 8, and 10 photons in lowest order.

gated the transition rates in the context of a physical picture which does not employ a perturbation expansion involving photons. Consider a $J \rightarrow J+1$ atom confined to a circularly polarized antinode. The atom is optically pumped into the outermost Zeeman component of its ground state and thus can be approximated by a two-level system. We can expand the light shift U of this ground state in powers of the Rabi frequency ω_1 (which is proportional to the square root of the total light intensity) in the vicinity of an antinode $\omega_1 = \omega_{1\max}$ which leads to a series of different powers $(\omega_1^2 - \omega_{1\max}^2)^n$. Assume now that the total light field consists of two parts: a circularly polarized one-dimensional optical standing wave of frequency ω_L which extends parallel to the x axis and which is described by its corresponding Rabi frequency $\omega_{\max} \times \cos(kx)$ ($k \equiv$ wave number) and the probe wave of frequency $\omega_L + \Delta$ and Rabi frequency ω_{probe} having the same polarization and propagating along the x direction. We may insert the corresponding total Rabi frequency ω_1 into the power expansion of the light shift and write $U = U_0 + U_\Delta + U_{2\Delta} + \ldots$ as a sum of quantities each collecting the terms which oscillate with the same frequency $n\Delta$, $n = 0,1,2,\ldots$. The term U_0 is then expanded with respect to x in the vicinity of an antinode yielding a harmonic oscillator potential to lowest order which gives rise to equidistant vibrational states. If we denote the vibrational states by $|i\rangle$, $i = 0,1,\ldots$ we may calculate the Rabi frequencies $\omega_{ij}(n)$ corresponding to the transitions between states $|i\rangle$ and $|j\rangle$ with respect to the perturbations $U_{n\Delta}$, $n = 1,2,\ldots$. If the Lamb-Dicke parameter $g \equiv (h\nu/2E_R)^{1/2}$ is sufficiently larger than 1 ($h\nu \equiv$ energy separation between adjacent vibrational levels, $E_R \equiv$ photon recoil energy) we find

$$\omega_{01}(n) = c_n g^{-1} (\omega_{1\max}\omega_{\text{probe}})^n \Omega_{\max}^{(1-2n)}$$

for transitions between the two lowest states [$\Omega_{\max} \equiv (\delta^2 + \omega_{1\max}^2)^{1/2}$]. The coefficient c_n contains a spatial integral including the wave functions of $|0\rangle$ and $|1\rangle$ and decreases rapidly with increasing n. The laser light intensities and the detuning used in our experiment ($\omega_{1\max}/\Gamma = 6$, $\delta/\Gamma = -8$, $\omega_{\text{probe}}/\Gamma = 0.3$, $g = 4.7$) lead to $\omega_{01}(1)/2\pi \approx 85$ kHz, $\omega_{01}(2)/2\pi \approx 0.75$ kHz, and $\omega_{01}(3)/2\pi \approx 10$ Hz. The value of 85 kHz is responsible for the power broadened linewidth of the first Raman sidebands at ± 165 kHz seen in the spectrum of Fig. 3(a). A two-level calculation including the states $|0\rangle$ and $|1\rangle$ yields the polarization $P_{01}(n,\Delta)$ connected with the Rabi frequency $\omega_{01}(n)$. The modification $dI_{01}(n,\Delta)$ of the probe intensity due to the $(n-1)$st subharmonic resonance should scale as the product of $P_{01}(n,\Delta)$ and the probe field, i.e.,

$$dI_{01}(n,\Delta) \sim \frac{\omega_{01}(n)\omega_{\text{probe}}}{\frac{1}{2}\gamma^2 + 2(\Delta-\omega)^2 + \omega_{01}(n)^2} \qquad (1)$$

(γ is the sum of the relaxation rates of $|0\rangle$ and $|1\rangle$ and $\omega \equiv 2\pi\nu$). We obtain $dI_{01}(1,\omega) = 12 dI_{01}(2,\omega)$ and $dI_{01}(2,\omega) = 77 dI_{01}(3,\omega)$. Experimentally we observe amplitude ratios between adjacent subharmonic sidebands of roughly 10 to 20; i.e., the predictions of our simplified model show the correct order of magnitude. Our model underestimates the strength of higher subharmonic sidebands, i.e., the coefficients c_n should decrease less rapidly with increasing n compared to what our model predicts.

We believe that our model could be improved if we account for higher lying vibrational levels. For higher lying levels transitions with small n (e.g., $n = 1$) might be suppressed relative to those with larger n (e.g., $n = 2$ or 3) because the rapidly oscillating wave functions at high vibrational quantum number j can only be efficiently coupled by a perturbation $U_{n\Delta}$ oscillating with comparable spatial period. In particular, because in three dimensions the jth vibrational level has $[(j+1)(j+2)/2]$-fold approximate degeneracy and because transitions between high lying (less localized) levels are less suppressed by the Lamb-Dicke effect, the contribution of the higher lying levels in the observed spectra might play an important role. More precise calculations should also use more realistic wave functions as calculated by taking into account the anharmonic terms of the optical potential. Actually, the two-level optical potential used in our model might not be appropriate at all when higher lying states are considered. When we move away from some antinode, say with clockwise circular polarization, the counterclockwise circular polarization component increases. Because the admixture of other than the outermost Zeeman state in the most light-shifted level is also increasing we expect a considerable additional light shift away from the antinodes as compared to the results of a two-level calculation which leads to extra anharmonicity.

In summary we have observed novel spectral features occurring at subharmonic frequencies in probe transmission spectra of cold atoms trapped in the antinodes of a three-dimensional optical standing wave. We have interpreted these features in terms of Raman transitions which involve multiple pairs of photons. We also have presented a high resolution spectrum of a sub-kHz Rayleigh resonance. Our experiment uses a body-centered-cubic optical lattice with ferromagnetic order of the atomic spins.

[1] P. Verkerk, B. Lounis, C. Salomon, C. Cohen-Tannoudji, J. Courtois, and G. Grynberg, Phys. Rev. Lett. **68**, 3864 (1992).

[2] P. Jessen, C. Gerz, P. Lett, W. Phillips, S. Rolston, R. Spreeuw, and C. Westbrook, Phys. Rev. Lett. **69**, 49 (1992).

[3] G. Grynberg, B. Lounis, P. Verkerk, J. Courtois, and C. Salomon, Phys. Rev. Lett. **70**, 2249 (1993).

[4] A. Hemmerich and T. Hänsch, Phys. Rev. Lett. **70**, 410 (1993).

[5] A. Hemmerich, C. Zimmermann, and T. Hänsch, Europhys. Lett. **22**, 89 (1993).

[6] A. Hemmerich and T. Hänsch, Phys. Rev. A **48**, R1753 (1993).

[7] J. Courtois and G. Grynberg, Phys. Rev. A **46**, 7060 (1992).